Electronic Supplementary Material

Self-supported porous heterostructure WC/WO_{3-x} ceramic electrode for hydrogen evolution reaction in acidic and alkaline media

Feihong WANG[a], Binbin DONG[b], Junwei WANG[c], Nianwang KE[a], Chuntian TAN[a], Anding HUANG[a], Yutong WU[a], Luyuan HAO[a], Liangjun YIN[d], Xin XU[a,*], Yuxi XIAN[e,*], Simeon AGATHOPOULOS[f]

[a]*CAS Key Laboratory of Materials for Energy Conversion, Department of Materials Science and Engineering, University of Science and Technology of China, Hefei 230026, China*

[b]*School of Materials Science and Engineering, Henan Key Laboratory of Special Protective Materials, Luoyang Institute of Science and Technology, Luoyang 471023, China*

[c]*Yangtze Delta Region Institute (Huzhou), University of Electronic Science and Technology of China, Huzhou 313001, China*

[d]*School of Energy Science and Engineering, University of Electronic Science and Technology of China, Chengdu 611731, China*

[e]*CAS Key Laboratory of Mechanical Behaviors and Design of Materials, Department of Modern Mechanics, University of Science and Technology of China, Hefei 230026, China*

[f]*Department of Materials Science and Engineering, University of Ioannina, Ioannina GR-451 10, Greece*

* Corresponding authors.

E-mail: X. Xu, xuxin@ustc.edu.cn

Y. Xian, yxxian@ustc.edu.cn

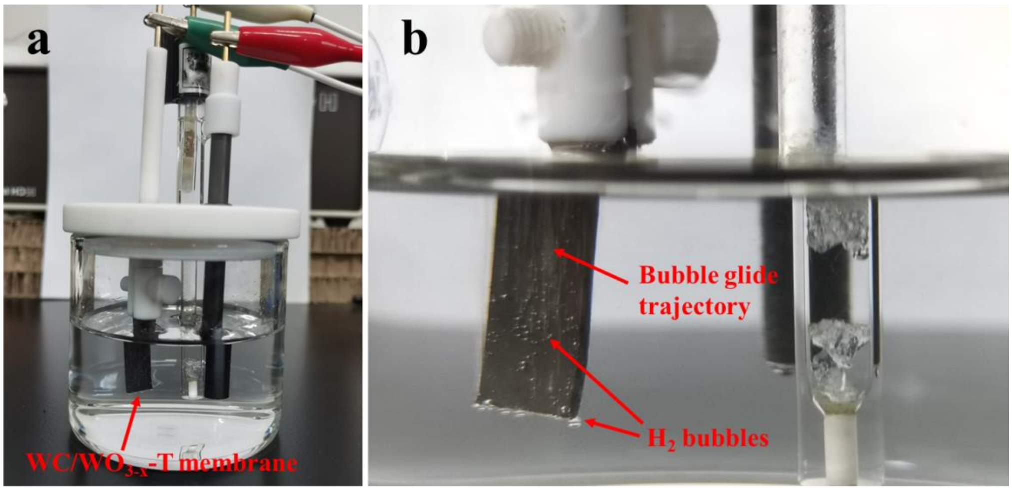

Fig. S1 Electrochemical test device. (a) Full view and (b) (detail of) the H_2 evolved from the electrode.

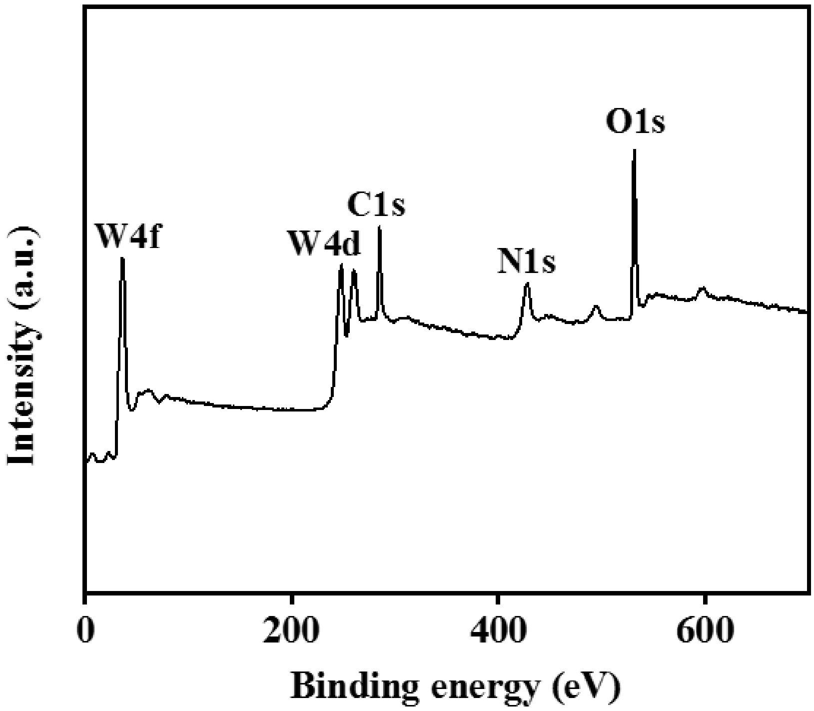

Fig. S2 XPS full spectrum of WC/WO_{3-x}-900.

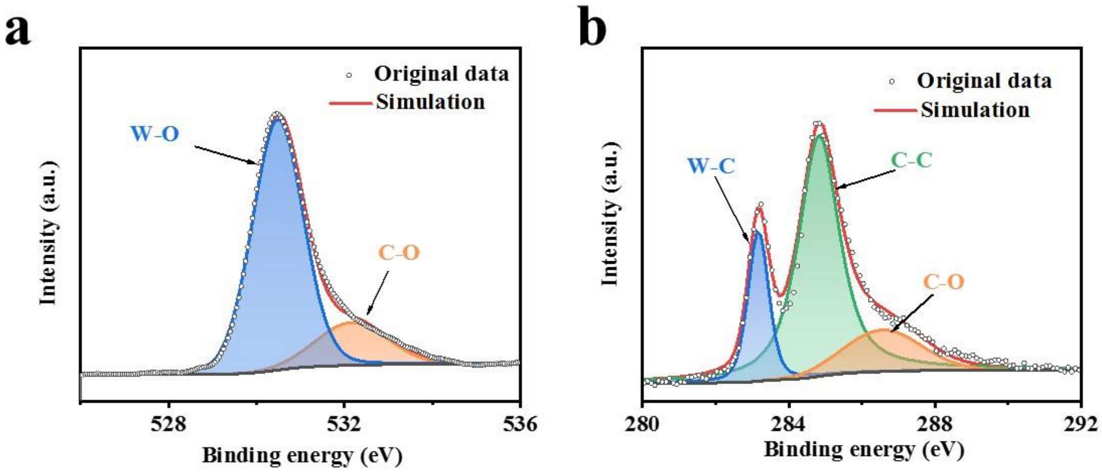

Fig. S3 High-resolution XPS spectra of (a) O 1s and (b) C 1s for the WC ceramic membrane.

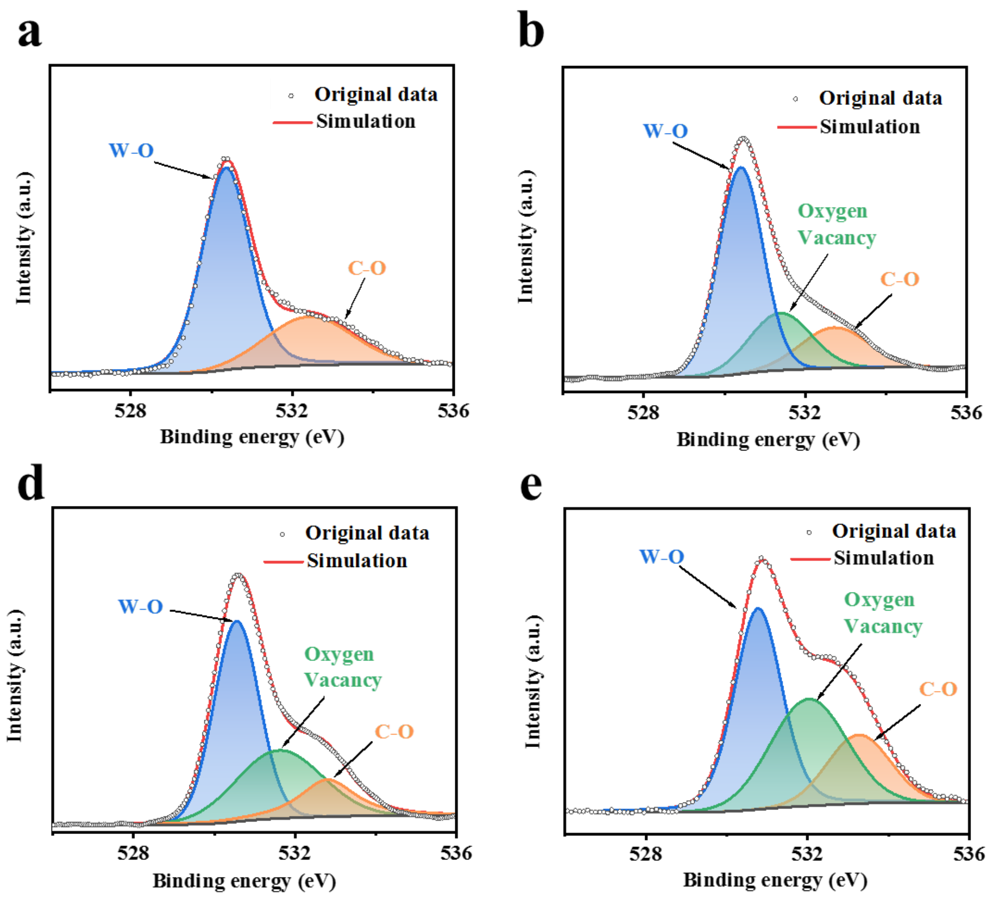

Fig. S4 High-resolution XPS spectra of O 1s for (a) WC/WO$_{3-x}$-700, (b) WC/WO$_{3-x}$-800, (c) WC/WO$_{3-x}$-900, and (d) WC/WO$_{3-x}$-1000.

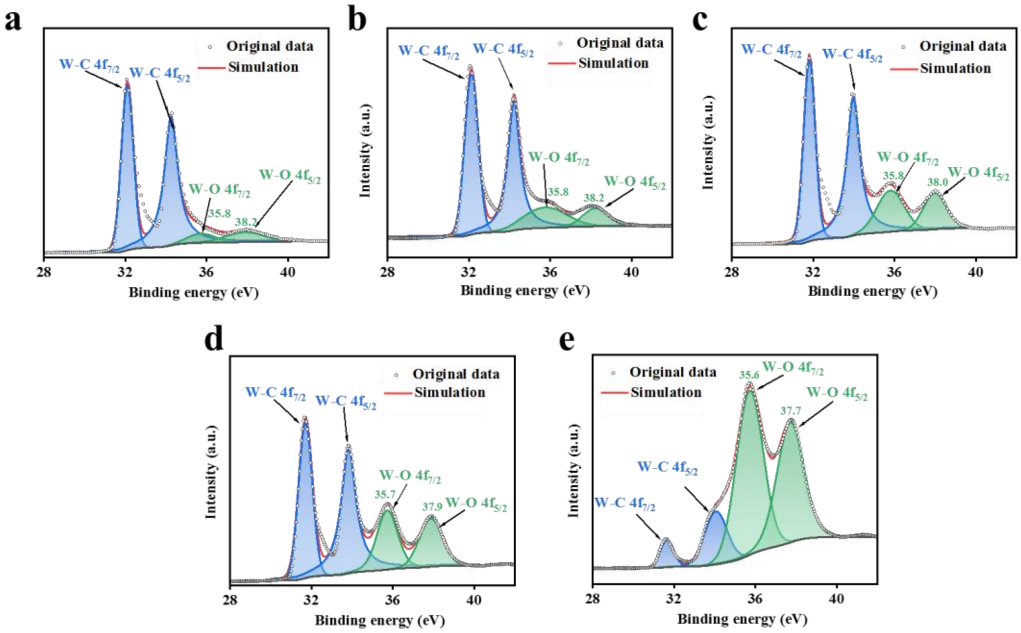

Fig. S5 High-resolution XPS spectra of W 4f for (a) WC, (b) WC/WO_{3-x}-700, (c) WC/WO_{3-x}-800, (d) WC/WO_{3-x}-900, and (e) WC/WO_{3-x}-1000.

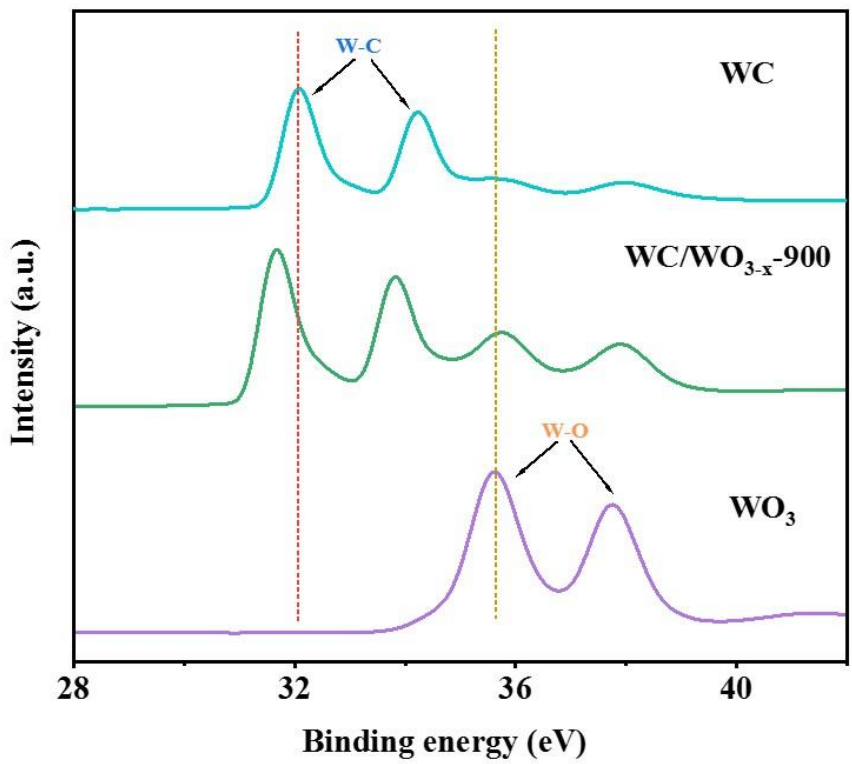

Fig. S6 High-resolution XPS spectra of W 4f for WC, WC/WO_{3-x}-900, and WO_3.

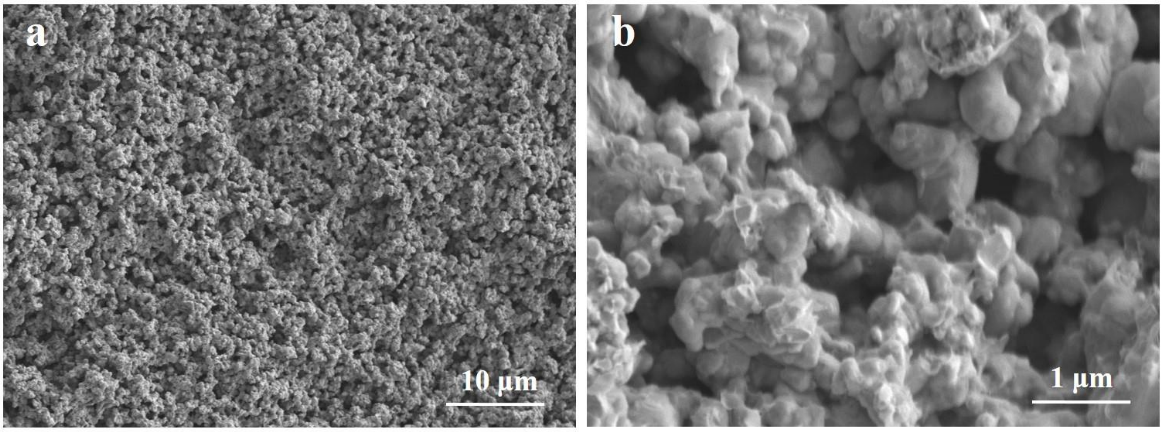

Fig. S7 Morphology of the fracture surface of WC ceramic membrane at (a) low and (b) high magnification.

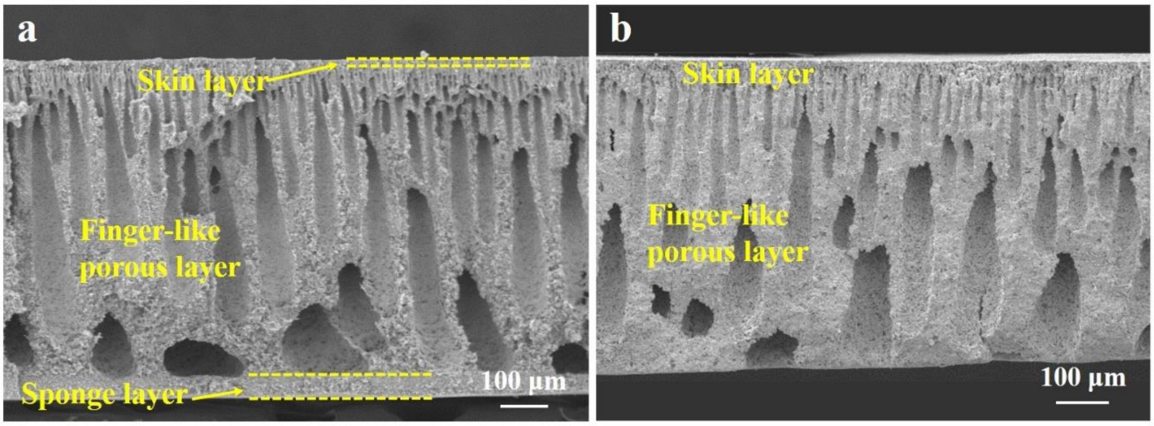

Fig. S8 Cross-section of (a) the green WC ceramic membrane and (b) after thermal treatment at 1600 °C in Ar atmosphere.

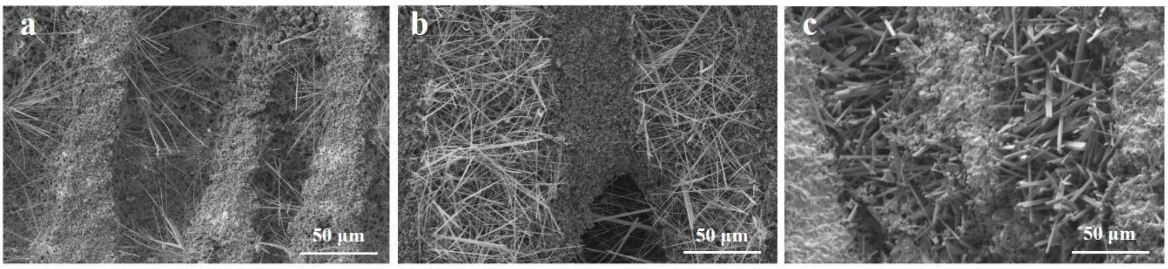

Fig. S9 Top view of (a) WC/WO_{3-x}-700, (b) WC/WO_{3-x}-800, and (c) WC/WO_{3-x}-1000.

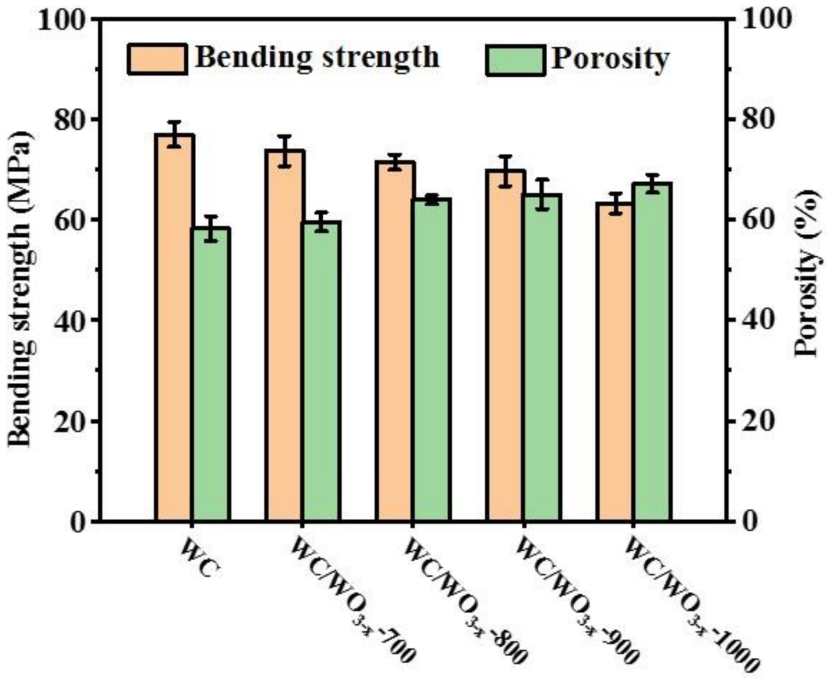

Fig. S10 Bending strength and porosity of WC and WC/WO_{3-x}-T.

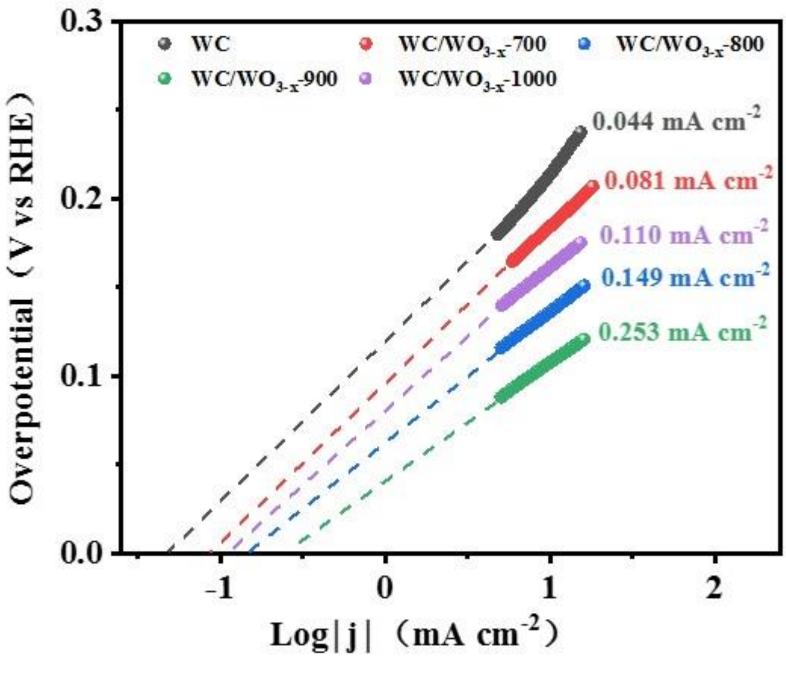

Fig. S11 Estimation (by extrapolation) of the exchange current density (j_0) (of HER) in 0.5 M H_2SO_4 media for WC and WC/WO_{3-x}-T.

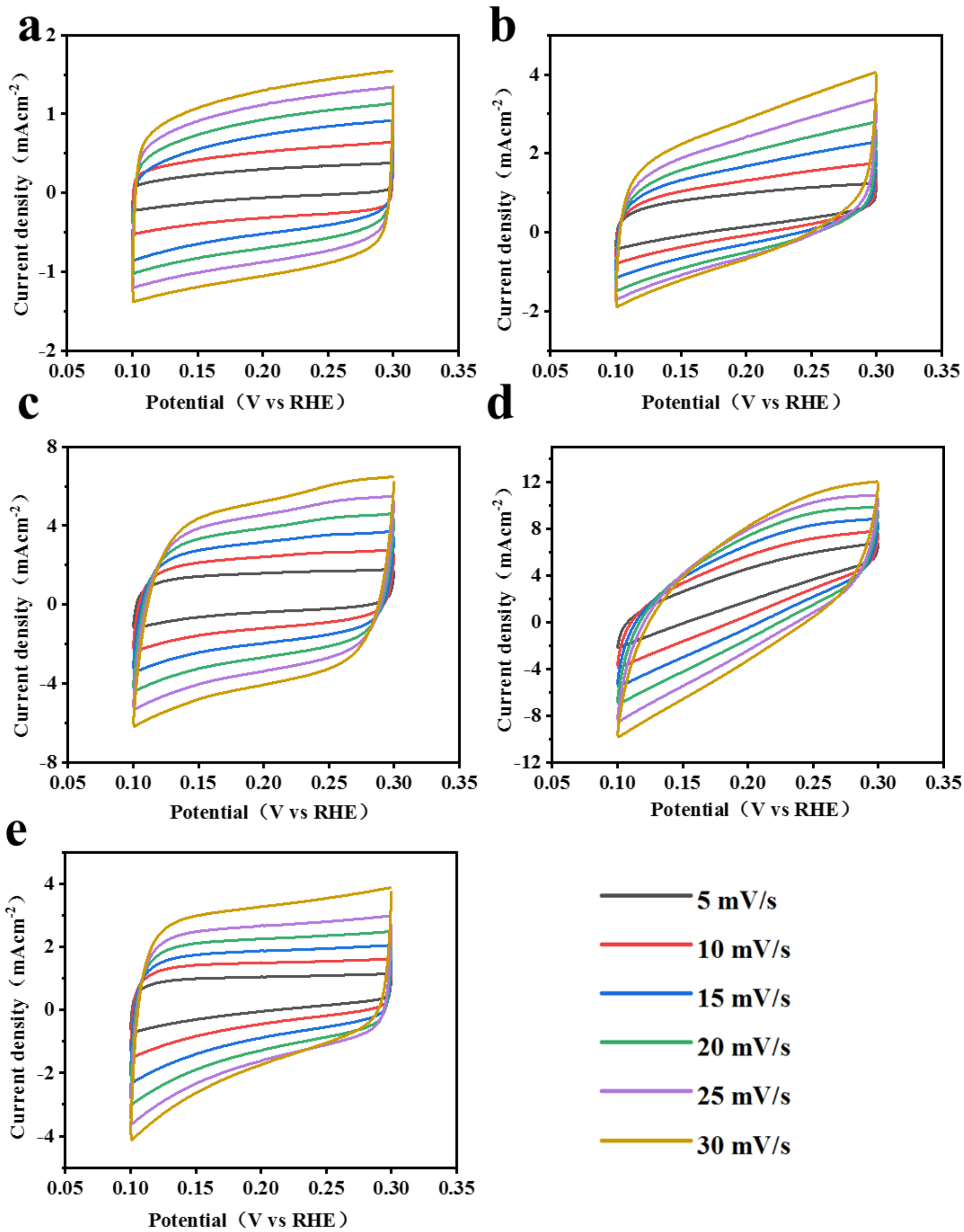

Fig. S12 CV curves of (a) WC, (b) WC/WO_{3-x}-700, (c) WC/WO_{3-x}-800, (d) WC/WO_{3-x}-900, and (e) WC/WO_{3-x}-1000 for evaluating the C_{dl} in 0.5 M H_2SO_4 media.

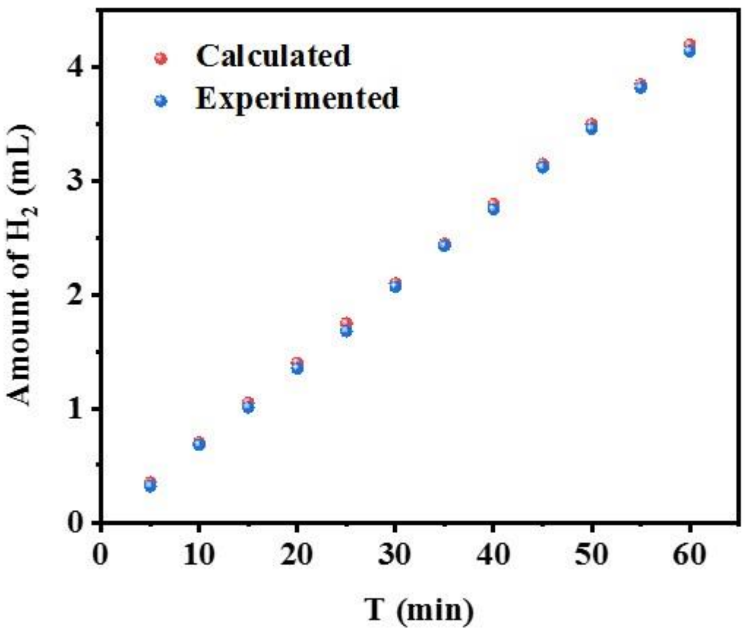

Fig. S13 Faradaic efficiency of WC/WO_{3-x}-900 in 0.5 M H_2SO_4.

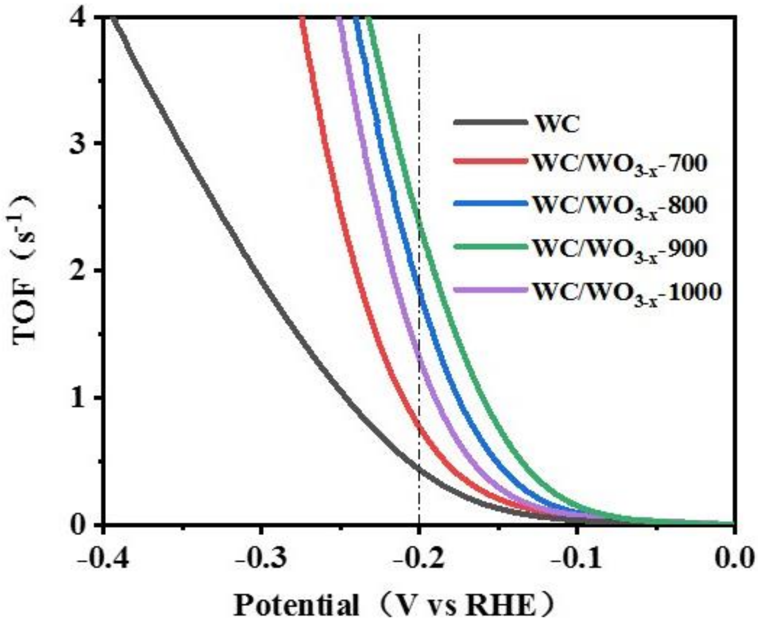

Fig. S14 Turnover frequency (TOF) of WC and WC/WO_{3-x}-T in 0.5 M H_2SO_4.

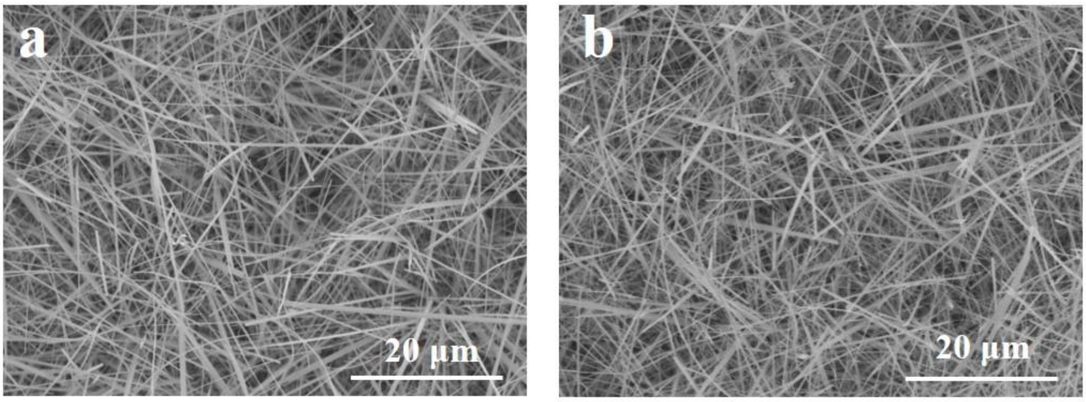

Fig. S15 Microstructure of WC/WO_{3-x}-900 after stability tests in (a) 0.5 M H_2SO_4 and (b) 1.0 M KOH.

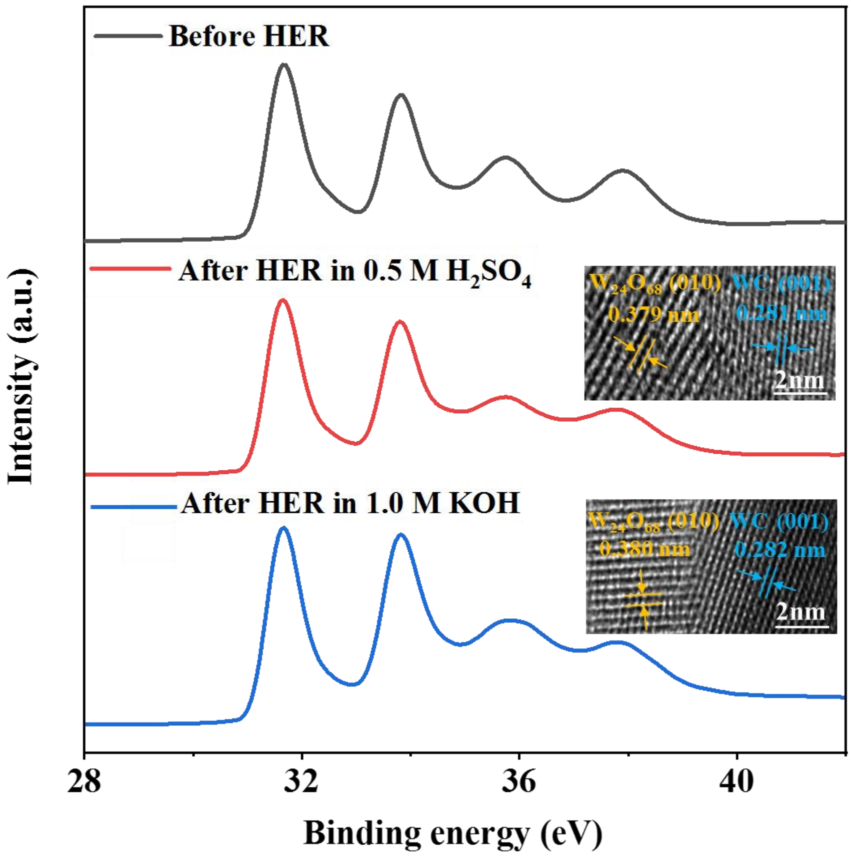

Fig. S16 W 4f XPS spectra and TEM (the insets) of WC/WO_{3-x}-900 before and after stability tests in 0.5 M H_2SO_4 and 1.0 M KOH.

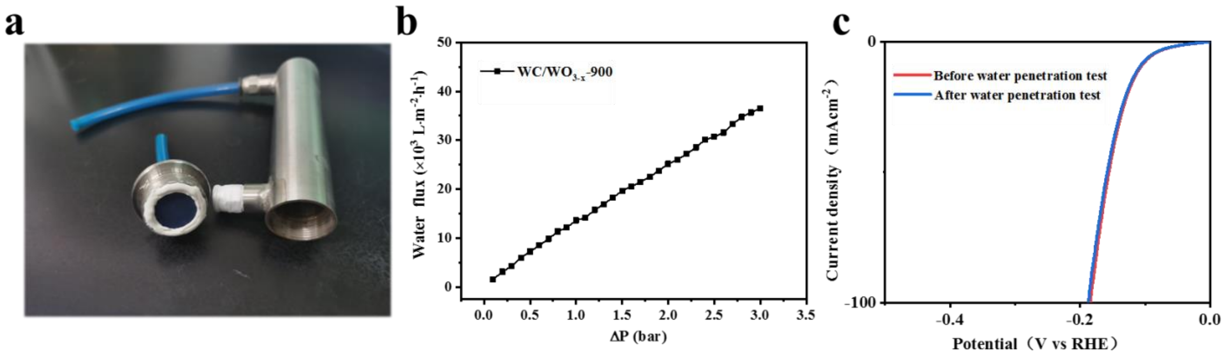

Fig. S17 Water permeability test. (a) Test device, (b) water permeability curve, and (c) LSV curves of WC/WO_{3-x}-900 before and after 4 h penetration test in 0.5 M H_2SO_4.

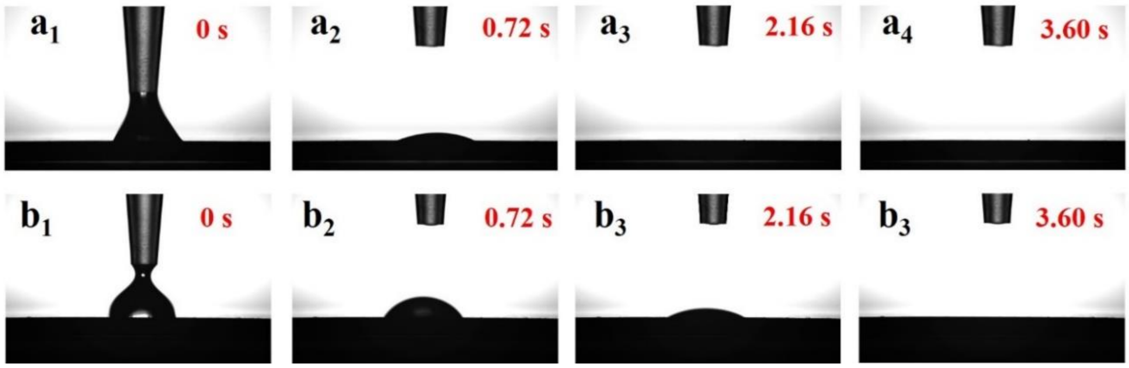

Fig. S18 Instants of water contact angle formed on WC/WO_{3-x}-900 over time in (a) 0.5 M H_2SO_4 and (b) 1.0 M KOH.

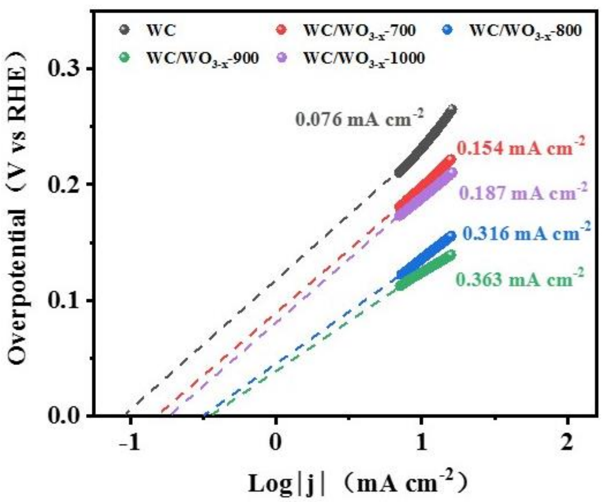

Fig. S19 Estimation (by extrapolation) of the exchange current density (j_0) (of HER) in 1.0 M KOH media for WC and WC/WO_{3-x}-T.

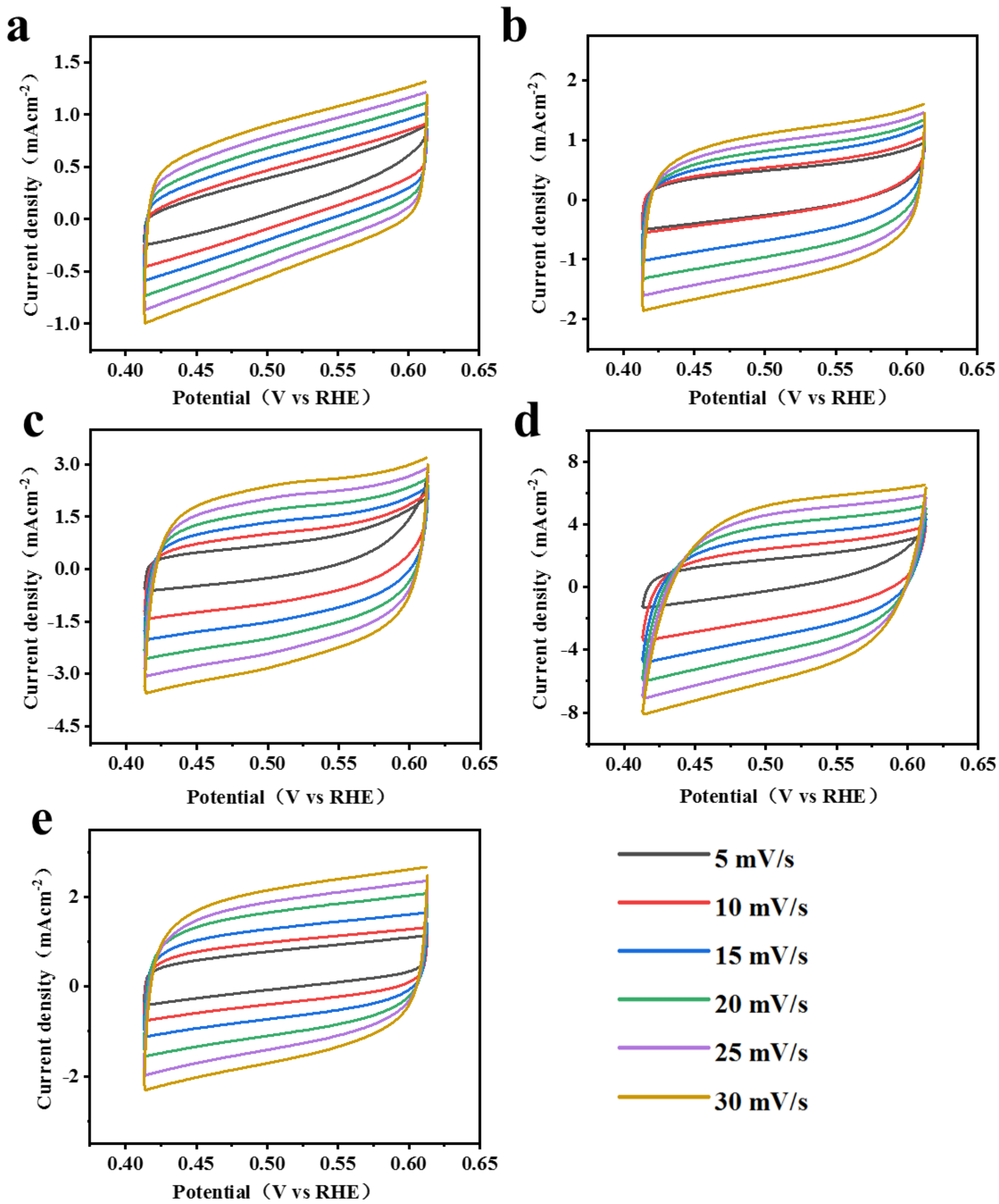

Fig. S20 CV curves of (a) WC, (b) WC/WO_{3-x}-700, (c) WC/WO_{3-x}-800, (d) WC/WO_{3-x}-900, and (e) WC/WO_{3-x}-1000 for evaluating the C_{dl} in 1.0 M KOH media.

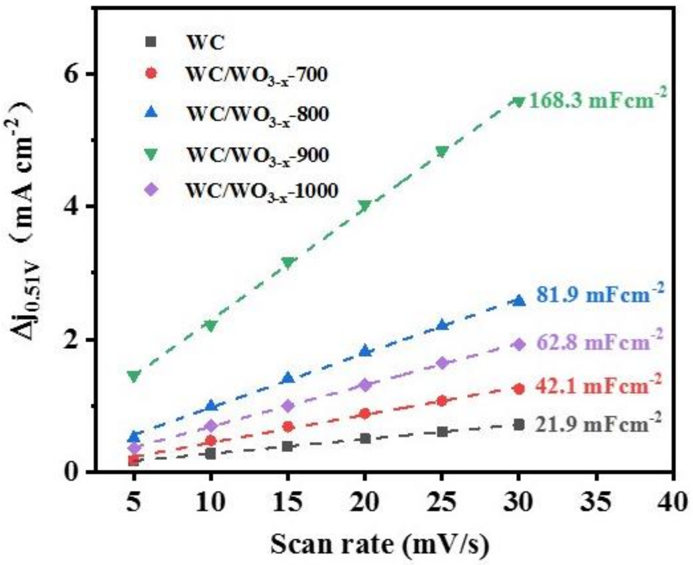

Fig. S21 C_{dl} values at a potential of 0.51 V (vs. RHE) of WC and WC/WO_{3-x}-*T* in 1.0 M KOH media.

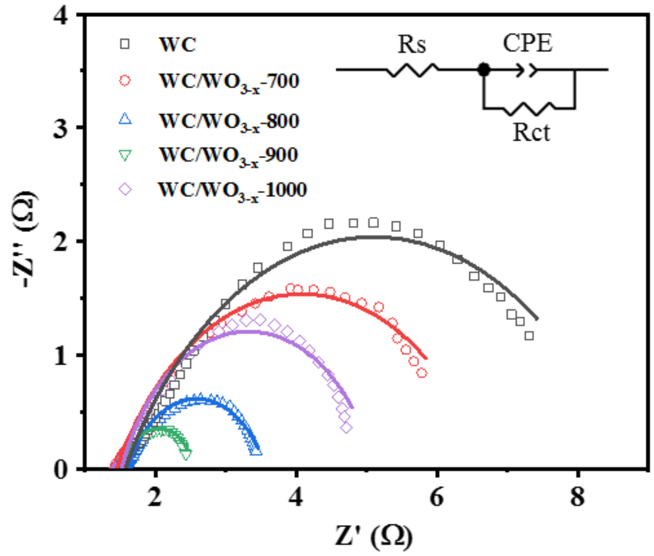

Fig. S22 Electrochemical impedance spectra (EIS) at an overpotential of 200 mV (the inset presents the equivalent circuit) in 1.0 M KOH media.

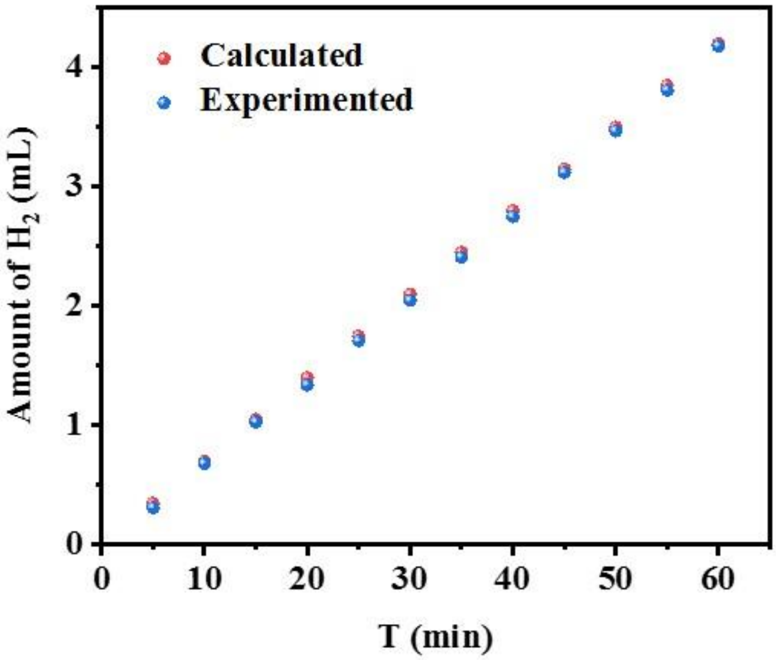

Fig. S23 Faradaic efficiency of WC/WO_{3-x}-900 in 1.0 M KOH media.

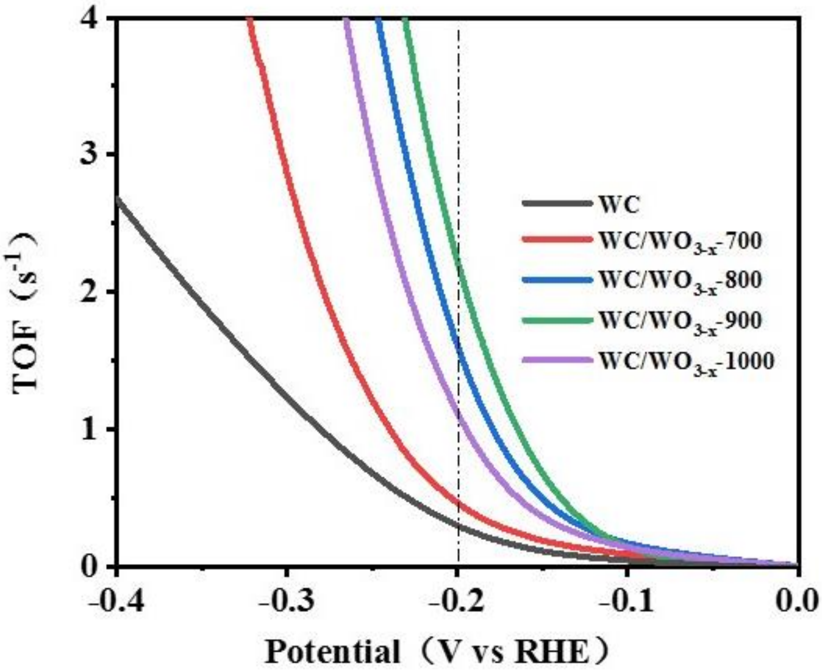

Fig. S24 Turnover frequency (TOF) of WC and WC/WO_{3-x}-*T* in 1.0 M KOH media.

Table S1 Compositions of the two slurries

Compound	Slurry composition (wt%)	
	WC slurry	Graphite slurry
N-methyl-2-pyrrolidone (NMP)	16.8	55.0
Polyethersulfone (PESf)	4.9	11.0
Polyvinylpyrrolidone (PVP)	1.0	1.7
WC powder	73.6	None
WO_3 powder	3.7	None
Graphite powder	None	32.3

Table S2 HER performance of WC and WC/WO_{3-x}-T in 0.5 M H_2SO_4 media

Sample	Overpotential (mV)	Tafel slope (mV dec^{-1})	C_{dl} (mF cm^{-2})	j_0 (mA cm^{-2})	R_{ct} (Ω)
WC	216	113.1	39.5	0.044	4.66
WC/WO_{3-x}-700	189	91.7	61.7	0.081	2.59
WC/WO_{3-x}-800	137	67.5	145.5	0.149	1.80
WC/WO_{3-x}-900	107	59.3	181.8	0.253	0.82
WC/WO_{3-x}-1000	161	73.5	78.2	0.110	1.94

Table S3 ECSA of WC and WC/WO_{3-x}-T in 0.5 M H_2SO_4 and 1.0 M KOH

Sample	A_{ECSA} (cm^2) 0.5 M H_2SO_4	A_{ECSA} (cm^2) 1.0 M KOH
WC	987.5	547.5
WC/WO_{3-x}-700	1542.5	1052.5

WC/WO_{3-x}-800	3637.5	2047.5
WC/WO_{3-x}-900	4545.0	4207.5
WC/WO_{3-x}-1000	1955.0	1570.0

Table S4 HER performance of WC and WC/WO_{3-x}-*T* in 1.0 M KOH media

Sample	Overpotential (mV)	Tafel slope (mV dec^{-1})	C_{dl} (mF cm^{-2})	j_0 (mA cm^{-2})	R_{ct} (Ω)
WC	234	140.3	21.9	0.076	6.92
WC/WO_{3-x}-700	198	115.8	42.1	0.154	5.25
WC/WO_{3-x}-800	136	93.2	81.9	0.316	1.95
WC/WO_{3-x}-900	123	72.4	168.3	0.363	1.01
WC/WO_{3-x}-1000	188	102.6	62.8	0.187	3.60

Table S5 Comparison of HER performance in 0.5 M H_2SO_4 media of the electrodes produced in the present study with other tungsten carbide-based catalysts previously reported in the literatures

Material	Overpotential (mV)	Tafel slope (mV dec^{-1})	Ref.
WC–CNTs	145	72	[S1]
W_2C NPs	123	45	[S2]
WC NPs	250	78	
2D WC	120	38	[S3]
W_2C@carbon	135	68	[S4]
W_2C microspheres	190	118	[S5]
W_xC@WS_2	146	61	[S6]
Cu@WC	92	50.5	[S7]

WC/Co@NCNTs	98	52	[S8]
N-doped WC	113	75	[S9]
Co_2P/WC@NC	91	40	[S10]
WC/WO_{3-x}-900	107	59.3	This work

Table S6 Comparison of HER performance in 1.0 M KOH media of the electrodes produced in the present study with other tungsten carbide-based catalysts previously reported in the literatures

Material	Overpotential (mV)	Tafel slope (mV dec^{-1})	Ref.
WC–CNTs	137	106	[S1]
2D i-WC–G	225	108	[S3]
Cu@WC	119	88.7	[S7]
W_2N/WC	148.5	47.4	[S11]
ES-WC/W_2C	75	59	[S12]
WC–W_2C/PNCDs	101	90	[S13]
Co–WC/CN	98	125	[S14]
Ni/WC	77	68.6	[S15]
CNS@WC/GF	68	72	[S16]
Mo_2C/W_2C	132	76	[S17]
WC/WO_{3-x}-900	123	72.4	This work

References

[S1] Fan XJ, Zhou HQ, Guo X. WC nanocrystals grown on vertically aligned carbon nanotubes: An efficient and stable electrocatalyst for hydrogen evolution reaction. *ACS Nano* 2015, **9**: 5125–5134.

[S2] Gong QF, Wang Y, Hu Q, *et al*. Ultrasmall and phase-pure W_2C nanoparticles for efficient electrocatalytic and photoelectrochemical hydrogen evolution. *Nat Commun* 2016, **7**: 13216.

[S3] Zeng MQ, Chen YX, Li JX, *et al*. 2D WC single crystal embedded in graphene for enhancing hydrogen evolution reaction. *Nano Energy* 2017, **33**: 356–362.

[S4] Zhou Y, Ma RG, Li PX, *et al*. Ditungsten carbide nanoparticles encapsulated by ultrathin graphitic layers with excellent hydrogen-evolution electrocatalytic properties. *J Mater Chem A* 2016, **4**: 8204–8210.

[S5] Ham DJ, Ganesan R, Lee JS. Tungsten carbide microsphere as an electrode for cathodic hydrogen evolution from water. *Int J Hydrogen Energ* 2008, **33**: 6865–6872.

[S6] Wang FM, He P, Li YC, *et al*. Interface engineered W_xC@WS_2 nanostructure for enhanced hydrogen evolution catalysis. *Adv Funct Mater* 2017, **27**: 1605802.

[S7] Yao MQ, Wang BJ, Sun BL, *et al*. Rational design of self-supported Cu@WC core–shell mesoporous nanowires for pH-universal hydrogen evolution reaction. *Appl Catal B Environ* 2021, **280**: 119451.

[S8] Ma RG, Song EH, Zhou Y, *et al*. Ultrafine WC nanoparticles anchored on co-encased, N-doped carbon nanotubes for efficient hydrogen evolution. *Energy Storage Mater* 2017, **6**: 104–111.

[S9] Han NN, Yang KR, Lu ZY, *et al*. Nitrogen-doped tungsten carbide nanoarray as an efficient bifunctional electrocatalyst for water splitting in acid. *Nat Commun* 2018, **9**: 924.

[S10] Gao Y, Lang ZL, Yu FY, *et al*. A Co_2P/WC nano-heterojunction covered with N-doped carbon as highly efficient electrocatalyst for hydrogen evolution reaction. *ChemSusChem* 2018, **11**: 1082–1091.

[S11] Diao JX, Qiu Y, Liu SQ, *et al*. Interfacial engineering of W_2N/WC heterostructures derived from solid-state synthesis: A highly efficient trifunctional electrocatalyst for ORR, OER, and HER. *Adv Mater* 2020, **32**: 1905679.

[S12] Chen ZG, Gong WB, Cong S, *et al*. Eutectoid-structured WC/W_2C heterostructures: A new platform for long-term alkaline hydrogen evolution reaction at low overpotentials. *Nano Energy* 2020, **68**: 104335.

[S13] Lu XF, Yu L, Zhang JT, *et al*. Ultrafine dual-phased carbide nanocrystals confined in porous nitrogen-doped carbon dodecahedrons for efficient hydrogen evolution reaction. *Adv Mater* 2019, **31**: 1900699.

[S14] Jin HY, Chen JY, Mao SJ, *et al*. Transition metal induced the contraction of tungsten carbide lattice as superior hydrogen evolution reaction catalyst. *ACS Appl Mater Interfaces* 2018, **10**: 22094–22101.

[S15] Ma YY, Lang ZL, Yan LK, *et al*. Highly efficient hydrogen evolution triggered by a multi-interfacial Ni/WC hybrid electrocatalyst. *Energy Environ Sci* 2018, **11**: 2114–2123.

[S16] Shen Y, Li L, Xi JY, *et al*. A facile approach to fabricate free-standing hydrogen evolution electrodes: Riveting tungsten carbide nanocrystals to graphite felt fabrics by carbon nanosheets. *J Mater Chem A* 2016, **4**: 5817–5822.

[S17] Ling Y, Kazim FMD, Zhang Q, *et al*. Construction of Mo_2C/W_2C heterogeneous electrocatalyst for efficient hydrogen evolution reaction. *Int J Hydrogen Energ* 2021, **46**: 9699–9706.